Tackling the evaporation rates of volatile HNS: A lab-scale experiment to serve marine pollution response

Laura Cotte

Centre of Documentation, Research and Experimentations on Accidental Water Pollution (Cedre), 715 rue Alain Colas, Brest, France

laura.cotte@cedre.fr

Ludovic Lepers

Royal Belgian Institute of Natural Sciences (RBINS), rue Vautier 29, Brussels, Belgium

llepers@naturalsciences.be

Sébastien Legrand

Royal Belgian Institute of Natural Sciences (RBINS), rue Vautier 29, Brussels, Belgium

slegrand@naturalsciences.be

Laurent Aprin

Laboratory for the Science of Risks (LSR), IMT Mines Ales, Ales, France

Laurent.Aprin@mines-ales.fr

Stéphane Le Floch

Cedre, 715 rue Alain Colas, Brest, France

stephane.le.floch@cedre.fr

ABSTRACT

Release of volatile Hazard Noxious Substances (HNS) at sea can lead to the formation of toxic, flammable or explosive gas plumes that can travel large distances and pose risks over a wide area in relatively short timescales. Yet, when an emergency is declared, key information regarding the short-term behavior of HNS is not available for responders. For volatile organic compounds (VOCs), one critical parameter that should be systematically predicted and/or assessed is the evaporation kinetics: this would warn first-responders against risks of gas clouds that might originate from the HNS slick. This paper presents new experimental data on the evaporation kinetics of several VOCs that were collected using the new Cedre's wind tunnel in the framework of the MANIFESTS[1] project. The air and liquid temperatures as well as the wind velocity profile were continuously monitored above the pool. The evaporation of each liquid was monitored following the weight loss fraction over time. The final objective was to assess mass fluxes at the sea-air interface and to compare it to analytical models. The evaporation process was generally highlighted by a sharp decrease in temperature of the liquid. At constant wind conditions, the mass flow rates were the highest for vinyl acetate, cyclohexane and acrylonitrile, and the lowest for petroleum benzine. Increasing wind velocities led to higher evaporation rates of chemicals, i.e. a faster evaporation of the slick. These new data were finally compared to the OSERIT (Oil Spill Evaluation and Response Integrated Tool) – Evaporation module developed in MANIFESTS and will contribute to the improvement of the prediction accuracy of existing evaporation models. This will offer crisis management stakeholders more precise information regarding the formation of toxic gas clouds (Go/No Go decision).

[1] MANIFESTS (MANaging risks and Impacts From Evaporating and gaseous Substances To population Safety) is co-funded by the European Union Civil Protection Mechanism of DG-ECHO (call UCPM-2020-PP-AG – Prevention and preparedness for marine pollution at sea and on shore.

INTRODUCTION

Maritime transport represents more than 80% of the international trade volume (UNCTAD, 2017). Apart from crude oil, tanker trades of refined petroleum products, chemicals and gas have increased by 4% over the 2019-2021 period, with a 5.6% growth in Liquefied Natural Gas (LNG) trade (UNCTAD, 2022). The volume of hazardous and noxious substances (HNS) is thus constantly rising with an increased risk of accidental spillages potentially associated with marine pollutions, whether in ports or in the open sea. In the event of an incident and a spill in the environment, information on the fate of the chemical(s) involved is essential to better anticipate the risks incurred by responders and populations, the impacts on the environment as well as the appropriate response techniques (Mamaca et al., 2009).

Chemicals accidentally spilled into the marine or aquatic environment generally undergo physical-chemical modifications that will characterize their behavior and fate. As observed by Mamaca et al. (2004) and Le Floch et al. (2011), these modifications are dependent on the intrinsic parameters of the product involved, the *in-situ* environmental parameters (temperature, density and salinity of the water) and the meteo-ocean conditions (e.g. sea state, wind speed, marine currents). A few hours following the spill, short-term effects may thus occur such as spreading, emulsification, natural dispersion in the water column, dissolution, and evaporation into the atmosphere. Longer term degradation (e.g. oxidation, biodegradation) and sedimentation processes can then follow, depending on the persistence and the nature of the substance.

One of the main concern is that around 2,000 different types of HNS are regularly shipped in bulk or package forms (Purnell, 2009) which thus make difficult to capture their behavior if accidentally released in the environment. Of the wide variety of HNS traded, volatile and gaseous substances

are particularly problematic for marine pollution response authorities. The release of such substances at sea can indeed lead to the formation of toxic, flammable or explosive gas plumes – sometimes invisible to the naked eye – that can travel large distances and pose risks over a wide area in relatively short timescales. Yet, key information on the risks that responders or rescue teams could take when intervening, or those that could impact coastal communities and the environment when allowing a shipping casualty to dock at a place of refuge remain poorly-known. The MANIFESTS EU-project is part of this context. The aim of the present study was to enhance knowledge of the mechanisms involved in the evaporation of a chemical from a slick on the water surface through a series of experimental tests at various scales. The present work was carried out at Cedre facilities, focusing on four HNS. The study involved characterizing the influence of wind speed on evaporation kinetics, using a wind tunnel developed during the MANIFESTS project. The vapor mass flow rate from the water surface to the air were then calculated. The experimental data collected on evaporation were then compared with predictions from the OSERIT – Evaporation module developed by RBINS in the framework of MANIFESTS.

METHODS

1. Chemicals

The list of chemicals studied is provided in Table 1. Selection was based upon their SEBC (Standard European Behavior Classification) behavior, the frequency of transport and the potential hazards associated with transport and storage, as well as the risks for human health. Chemicals identified as ‘evaporators’ (E) (Bonn Agreement 1994) in their short-term fate were given priority. All chemicals studied were of analytical grade.

Table 1. List of HNS studied in the lab (from https://manifests-project.eu/hns-database/).

Chemicals	CAS number	SEBC	Boiling point* (°C)	Vapor pressure (kPa) at 20°C*
Acrylonitrile	107-13-1	DE	77.4	11.5
Cyclohexane	110-82-7	E	80.7	10.3
Petroleum benzine	64742-82-1	FE	90	3 – 3.3
Vinyl acetate	108-05-4	ED	72.7	12.0

2. Evaporation kinetic: wind tunnel set up

The evaporation kinetics of each chemical was investigated using a wind tunnel developed by Cedre in the framework of the MANIFESTS project. The aim of wind tunnel evaporation tests is to characterize the influence of wind speed on the evaporation rate of chemicals (pure or mixtures). This entails establishing a straight air flow with fully controlled mean speed and velocity profile. The air velocity profile corresponds to the variation of horizontal wind speed and direction with height, i.e. from the ground or the sea surface – where the wind speed is null – to the atmospheric boundary layer where the 'maximum' speed is reached (e.g. Jones et al. 1971). Such velocity profile depends on the roughness of the terrain over which the wind blows and directly impacts material transfer mechanisms at the surface of HNS slicks. Cedre has built a dedicated wind tunnel for this purpose. The experimental set up is displayed in Figure 1. It consisted of a 3000 $m^3.h^{-1}$ centrifugal hood fan with a cross-section of 25.4 cm x 29.2 cm positioned at the entrance of a plywood tunnel of approximately 4 m long. The fan speed was controlled using a frequency three-phase converter. A 30 cm-thick aluminum honeycomb (Euro-Composites) ensured that the air flow was homogenized with a fully developed turbulent flow. The honeycomb grid shape and porosity had to be selected carefully to mitigate at best the turbulence generated by the fan (Cattafesta et al., 2010; Decelle & Nicolas, 2017): a hexagonal grid with cell size of 6.4 mm appeared as a good compromise (Hamzah et al., 2021). An opening was integrated into the floor to accommodate tank

of various dimensions inside the tunnel, allowing for sizes up to 18 x 23 x 4 cm, with a capacity to evaporate 500 mL of product.

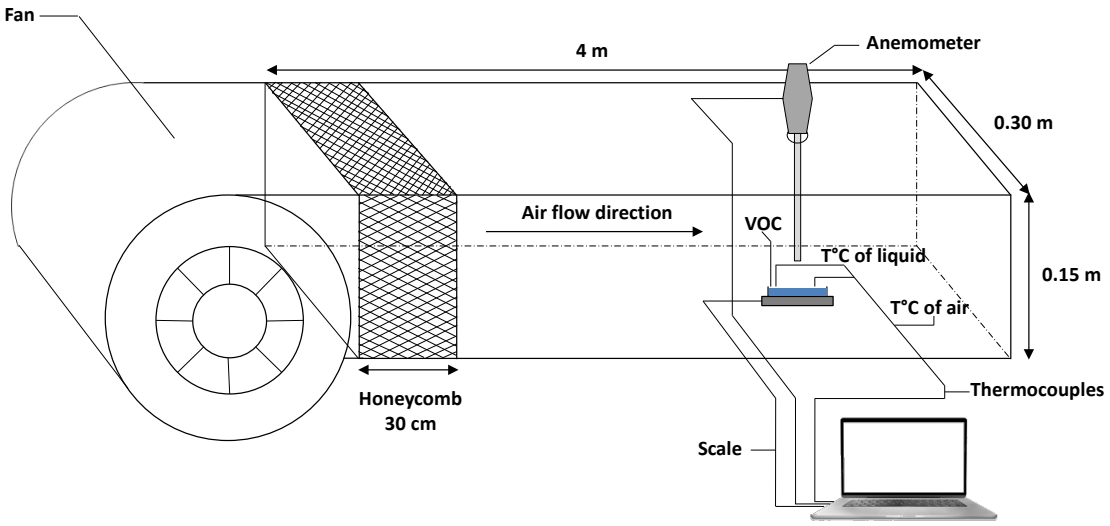

Figure 1. Diagram of the wind tunnel adapted from Heymes et al. (2013).

A petri dish containing 10 mL of pure chemical was positioned on top of the 0.001 g-precision scale (Mettler – Toledo XS1203S) inside the tunnel. The evaporation of the liquid was assessed by recording the mass loss of each chemical over time. The liquid and air temperatures were measured by three K-type thermocouples (Figure 2). Mass and temperature data were recorded in real time at 2 Hz and 1 Hz, respectively. The mean air flow speed was monitored using a hotwire anemometer (SEFRAM 9862) positioned at 10 cm above the petri dish. Experimental air flow velocities were chosen in the range of 0.5 – 11 $m.s^{-1}$ (0.5; 1; 2; 3, 4; 7; 8 and 11 $m.s^{-1}$). While no specific turbulence measurement was performed, the flow pattern was characterized by evaluating the dimensionless Reynolds number. This parameter depends on the wind velocity (U_{air}), the hydraulic diameter of the vein (d) and the kinematic viscosity of the air (ν_{air}), expressed as follows:

$$R_e = \frac{U_{air} \times d}{\nu_{air}}$$

In this case, Re was ranging from 6,300 to 190,000 which is typical of a turbulent flow in a tunnel.

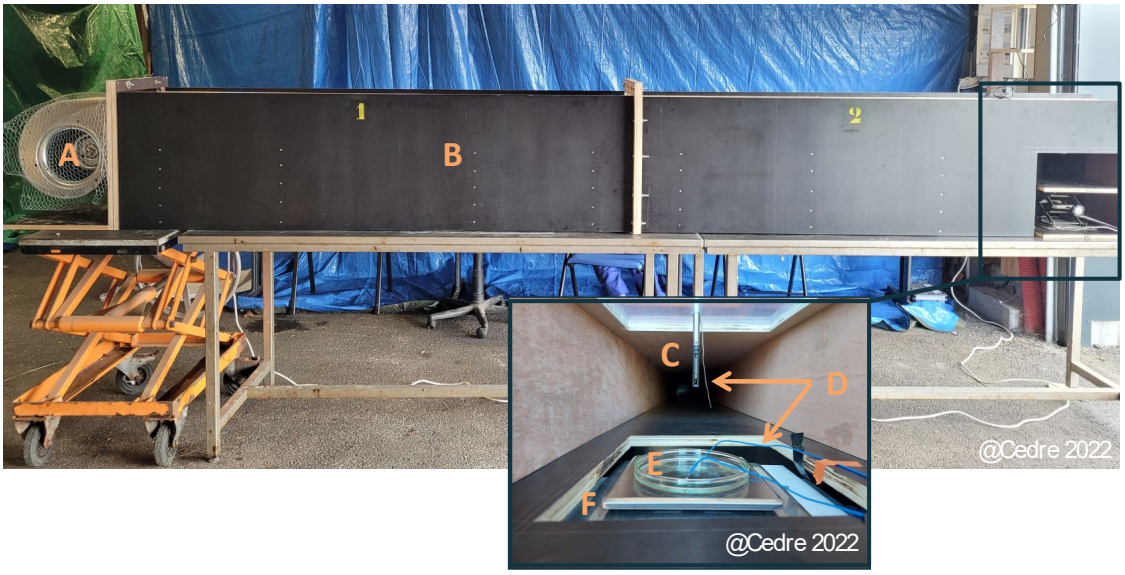

Figure 2. Panoramic view of the wind tunnel with a close-up image of the petri dish and the operating sensors inside the gallery: A) fan; B) tunnel; C) anemometer; D) thermocouples; E) petri-dish and F) weighing scale.

3. Modelling

The experimental data collected were used to assess the OSERIT model's capacity to simulate evaporation, dissolution and volatilization processes, as these three main processes have a significant impact on the atmospheric concentration of volatile HNS when accidentally released at sea (Lepers & Legrand 2022). Developed by RBINS, OSERIT is a multipurpose Lagrangian particles model able to simulate the trajectory of floating objects adrift at sea as well as the drift, fate, and behavior of acute marine pollution events by oil and other harmful and noxious substances (HNS) (Dulière et al., 2012; Legrand et al., 2017). The model uses external forcing from various

sources to simulate drift and atmospheric dispersion and considers several parameters, such as wind, wave, current, and temperature. Lagrangian particles move in a 3D space and are influenced by the value of the parameters at their location. For instance, airborne particles are affected solely by wind, while those at the surface are impacted by wind, current, and waves. In contrast, particles in the water column are only affected by current and waves. Additionally, there are many more factors at play, including turbulent kinetic diffusion and buoyancy (only for particles in the water). To compute the fate, the pollutant volume is equally divided between the different Lagrangian particles; the pollutant volume being itself subdivided at the level of a particle as a function of the chemical compound (or pseudo-compound). Each of the chemical compounds in the particle can be in several states: liquid (slick or droplets), emulsified, evaporated, dissolved, and degraded. The model is also able to simulate mixture, when they are non-azeotropic and there is no chemical reaction: each component of the mixture is treated as separated compounds. To track accurately the change of state of chemicals, the weathering module of OSERIT have been improved in the framework of the MANIFESTS project (Lepers & Legrand, 2022). It includes among other, evaporation, dissolution, and volatilization. Finally, because the state of chemical compounds influences the drift behavior of a Lagrangian particle, the pollutant mass is periodically redistributed between neighboring particles to minimize the number of different states active in each particle. This also assures the conservation of mass of the pollutant during the entire simulation. To start a simulation, the user must provide the physical-chemical properties of the HNS along with the meteorological forcing parameters such as wind, waves, and current. These data sources can be accessed from the HNS data base, the Copernicus Marine Service, and the European Centre for Medium-Range Weather Forecasts.

RESULTS/DISCUSSION

1. Experimental data on evaporation

Experiment at constant wind velocity

The first test consisted in monitoring the mass variation over time of acrylonitrile, cyclohexane, petroleum benzine and vinyl acetate under a constant wind of 8 $m.s^{-1}$ (Figure 3).

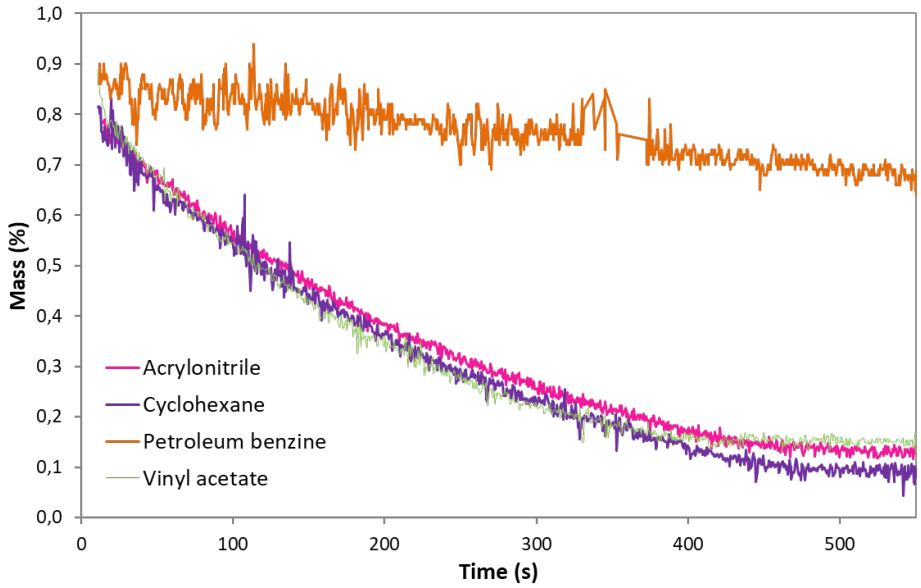

Figure 3. Evaporation of acrylonitrile, cyclohexane, petroleum benzine (PB) and vinyl acetate at constant wind velocity (8 $m.s^{-1}$). The experiment performed with PB last around 2 h.

Mass variation is similar for Acrylonitrile, cyclohexane and vinyl acetate with a polynomial law decrease whereas Petroleum benzine seems to decrease according to a linear law. After filling the petri-dish, a sharp decrease of liquid temperature in the range of 10-15°C was observed for acrylonitrile, cyclohexane and vinyl acetate (Figure 4). A small drop of around 2°C was also noticed for petroleum benzine when focusing on a narrow range of temperature (not shown). In this case, a higher measurement frequency could be useful to enhance temperature data resolution (e.g. 2 Hz).

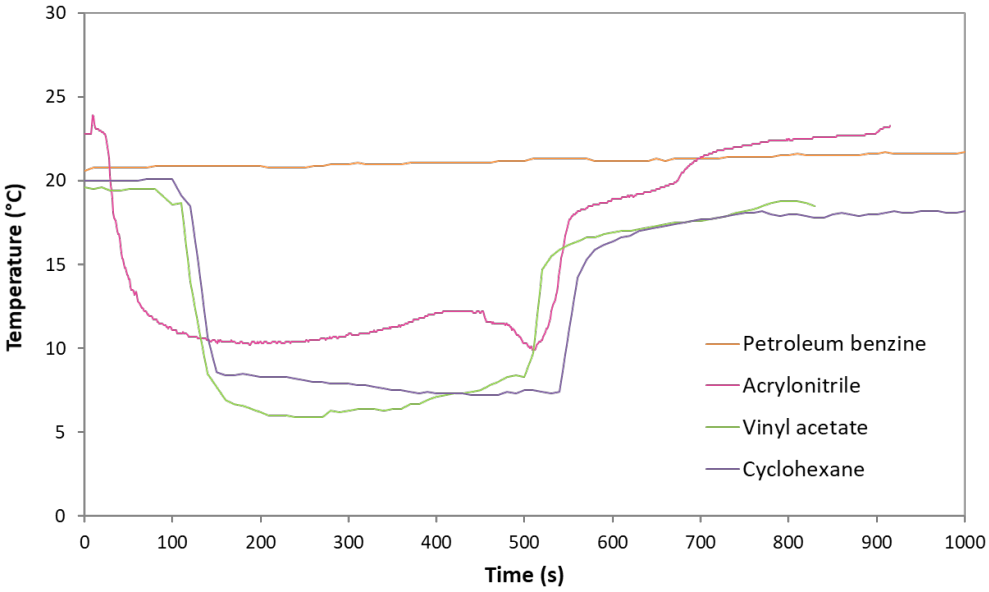

Figure 4. Liquid temperature over the evaporation process at constant wind velocities (8 $m.s^{-1}$).

Evaporation is an endothermic process that absorbs energy, or heat, from the environment, thus lowering the energy level of the medium (Gonczi, 2005). Here the heat loss was not compensated by sufficient heat exchange from the environment (air, solar intake, etc.). This transiently led to a drop in liquid temperature that tended to reduce vapor pressure and, hence, evaporation. This feature was already observed in previous works (e.g. Braconnier et al. 2008; Heymes et al. 2013). After 125 s for acrylonitrile, 160 s for cyclohexane 150 s for vinyl acetate and 2320 s (40 min) for petroleum benzine, the liquid temperature remained stable and the evaporation rate became constant (Figure 4). The mass flow rate was calculated according to Mackay and Matsugu 1973 model (Mackay & Matsugu, 1973) as described in (Cotte et al., 2023). Results are reported in Table 2. At constant wind conditions, the mass flow rates were the highest for vinyl acetate (19.22 $g.m^2.s^{-1}$), cyclohexane (14.27 $g.m^2.s^{-1}$) and acrylonitrile (11.91 $g.m^2.s^{-1}$) and the lowest for petroleum benzine (0.25 $g.m^2.s^{-1}$).

Table 2. Physical properties and mass transfer constants at a wind velocity of 8 $m.s^{-1}$.

Parameter	Acrylonitrile	Cyclohexane	Petroleum benzine	Vinyl acetate
Vapor pressure (kPa)	10,89	10,10	0,70	12,62
Vapor diffusion coefficient ($m^2.s^{-1}$)	$3,17 \times 10^{-5}$	$2,46 \times 10^{-5}$	$1,87 \times 10^{-6}$	$2,66 \times 10^{-5}$
Schmidt number	0,50	0,65	8,55	0,60
Mass transfer coefficient K_G ($m.s^{-1}$)	$4,98 \times 10^{-2}$	$4,09 \times 10^{-2}$	$8,11 \times 10^{-3}$	$4,33 \times 10^{-2}$
Mass flow J ($g.m^2.s^{-1}$)	11,91	14,27	0,25	19,22

Table 3. Physical properties and mass transfer constants at different wind velocities for acrylonitrile.

Parameter	Wind velocity ($m.s^{-1}$)							
	0.5	1	2	3	4	7	8	10
Average air temperature (K)	294,14	294,50	294,88	294,01	295,31	296,33	296,50	297,57
Average liquid temperature (K)	290,27	289,29	290,90	290,41	291,12	289,36	290,74	293,18
Kinematic air viscosity ($m^2.s^{-1}$) *	$1,6 \times 10^{-5}$	$1,6 \times 10^{-5}$	$1,6 \times 10^{-5}$	$1,6 \times 10^{-5}$	$1,6 \times 10^{-5}$	$1,6 \times 10^{-5}$	$1,6 \times 10^{-5}$	$1,6 \times 10^{-5}$
Vapor pressure (kPa)	12,66	12,86	13,08	12,59	13,33	13,93	14,04	14,69
Vapor diffusion coefficient ($m^2.s^{-1}$)	$4,81 \times 10^{-6}$	$1,31 \times 10^{-5}$	$1,84 \times 10^{-5}$	$2,25 \times 10^{-5}$	$2,62 \times 10^{-5}$	$3,12 \times 10^{-5}$	$3,17 \times 10^{-5}$	$3,31 \times 10^{-5}$
Schmidt number	3,33	1,22	0,87	0,71	0,61	0,51	0,50	0,48
Mass transfer coefficient K_G ($m.s^{-1}$)	$1,64 \times 10^{-3}$	$5,64 \times 10^{-3}$	$1,19 \times 10^{-2}$	$1,86 \times 10^{-2}$	$2,55 \times 10^{-2}$	$4,43 \times 10^{-2}$	$4,98 \times 10^{-2}$	$6,09 \times 10^{-2}$
Mass flow J ($g.m^2.s^{-1}$)	0,45	1,57	3,38	5,10	7,34	13,29	15,05	19,19

Table 4. Physical properties and mass transfer constants at different wind velocities for cyclohexane.

Parameter	Wind velocity ($m.s^{-1}$)							
	0.5	1	2	3	7	8	10	11
Average air temperature (K)	293,43	293,15	293,84	293,72	293,21	293,38	292,82	293,92
Average liquid temperature (K)	290,42	291,39	291,77	290,85	291,25	288,62	290,05	291,85
Kinematic air viscosity ($m^2.s^{-1}$)*	$1,6 \times 10^{-5}$	$1,6 \times 10^{-5}$	$1,6 \times 10^{-5}$	$1,6 \times 10^{-5}$	$1,6 \times 10^{-5}$	$1,6 \times 10^{-5}$	$1,6 \times 10^{-5}$	$1,6 \times 10^{-5}$
Vapor pressure (kPa)	10,13	9,99	10,32	10,26	10,02	10,10	9,85	10,36
Vapor diffusion coefficient ($m^2.s^{-1}$)	$6,36 \times 10^{-6}$	$1,24 \times 10^{-5}$	$1,68 \times 10^{-5}$	$2,34 \times 10^{-5}$	$2,85 \times 10^{-5}$	$2,46 \times 10^{-5}$	$2,40 \times 10^{-5}$	$2,52 \times 10^{-5}$
Schmidt number	2,51	1,29	0,95	0,68	0,56	0,65	0,67	0,63
Mass transfer coefficient K_G ($m.s^{-1}$)	$2,00 \times 10^{-3}$	$5,22 \times 10^{-3}$	$1,12 \times 10^{-2}$	$1,88 \times 10^{-2}$	$4,14 \times 10^{-2}$	$4,09 \times 10^{-2}$	$4,89 \times 10^{-2}$	$5,47 \times 10^{-2}$
Mass flow J ($g.m^2.s^{-1}$)	0,70	1,80	3,97	6,65	14,32	14,27	16,64	19,52

*Kinematic air viscosities are from Heymes et al. (2013).

Experiment at increasing wind velocities

The second test consisted in investigating the evaporation process of acrylonitrile and cyclohexane at increasing wind velocities in the range of 0.5 to 11 $m.s^{-1}$. Physical properties and mass flow rates are reported in Tables 3 and 4. Mass losses for acrylonitrile and cyclohexane versus time for different wind velocities are presented in Figure 5. A typical representation of the mass loss recorded at a specific wind velocity and coupled with the corresponding air and liquid temperature is also shown as an example (Figure 6). Acrylonitrile and cyclohexane generally presented a linear mass loss over time. Mass also decreased faster with increasing wind velocities as evidenced by steeper slopes (Figure 5). This suggests that an increase in wind velocity generally involves higher evaporation rates. Above the apparent thresholds of 7 $m.s^{-1}$ for acrylonitrile and 5 $m.s^{-1}$ for cyclohexane, the evaporation rate seemed to stagnate as the slopes did not seem anymore to increase proportionally with the wind velocity (Figure 5).

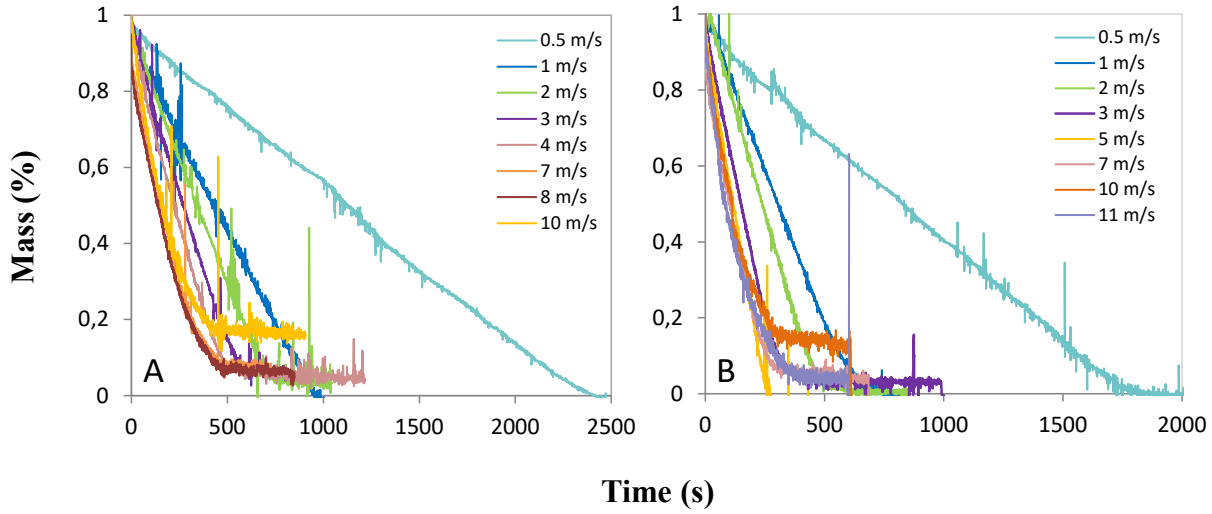

Figure 5. Evaporation rate of acrylonitrile (A) and cyclohexane (B) at various wind velocities.

A rapid saturation of the air with vapors of the chemical might partly explain this phenomenon. In addition, the evaporation process could have been hindered by the decrease of the slick area as well as the sharp decrease in temperature that was often greater than 10°C (e.g. Figure 7). In the case of cyclohexane, the temperature drop is such that it reaches a temperature close the cyclohexane's melting point (6.6°C). Cyclohexane crystals were indeed observed in the petri-dish at wind velocities ranging from 2 $m.s^{-1}$ to 11 $m.s^{-1}$ as the substance started to freeze (Figure 7).

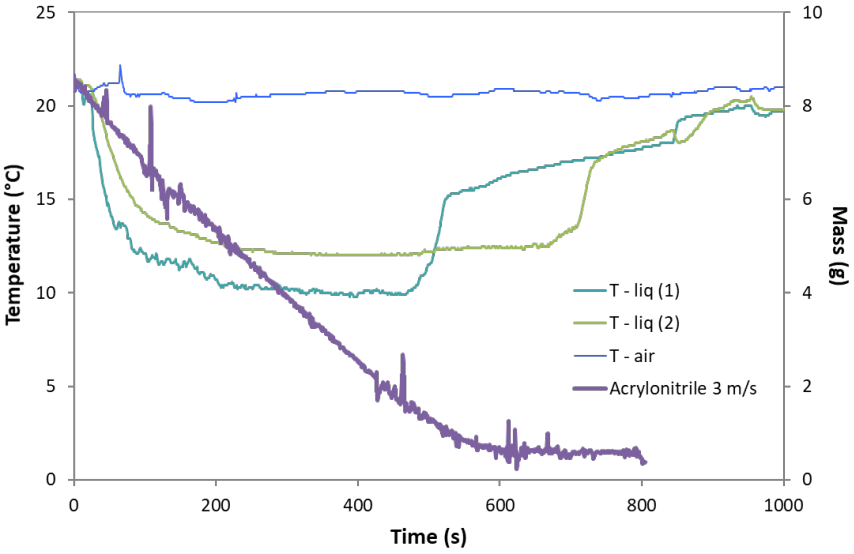

Figure 6. Evaporation of acrylonitrile at 3 $m.s^{-1}$ with associated air and liquid temperatures.

Surprisingly, the mass flow rates calculated do not reflect a clear 'stagnation' of the evaporation kinetics at high wind conditions (Figure 8). However, as observed by Bogeshwaran et al. (2015) for the diffusion of hexane in the air, increasing wind velocities clearly affects diffusion: the vapor diffusion coefficient increases up to a threshold value reached at stronger wind conditions (Figure 8). This suggests that the available space for diffusion is saturated by molecules of acrylonitrile or cyclohexane and that further changes in the factors influencing diffusion, such as temperature, wind speed, or concentration gradients, do not significantly alter anymore the diffusion coefficient. However, it is important to note that the diffusion coefficient alone does not dictate the rate of

evaporation. Additional information and consideration are thus needed to draw conclusions about the evaporation process itself.

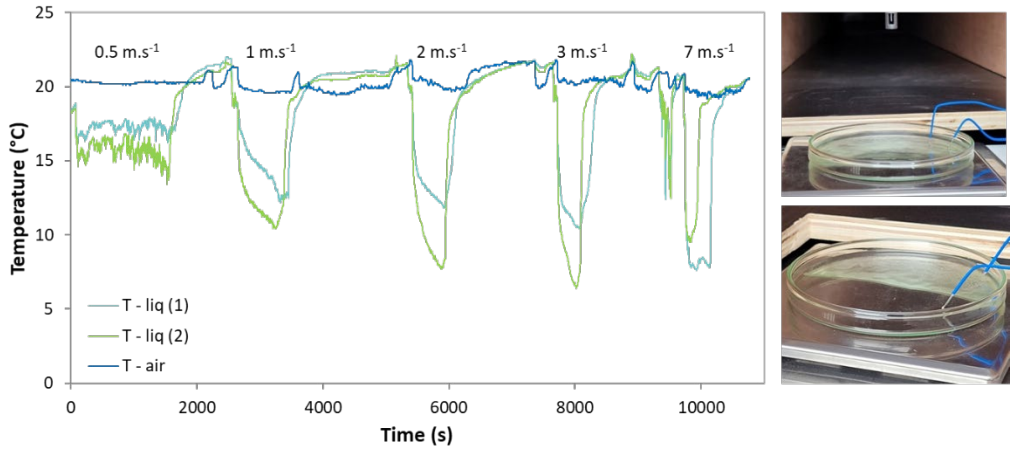

Figure 7. Air and liquid temperatures of cyclohexane at various wind velocities. Cyclohexane crystals can be observed in the petri-dish (right) as it starts freezing while evaporating.

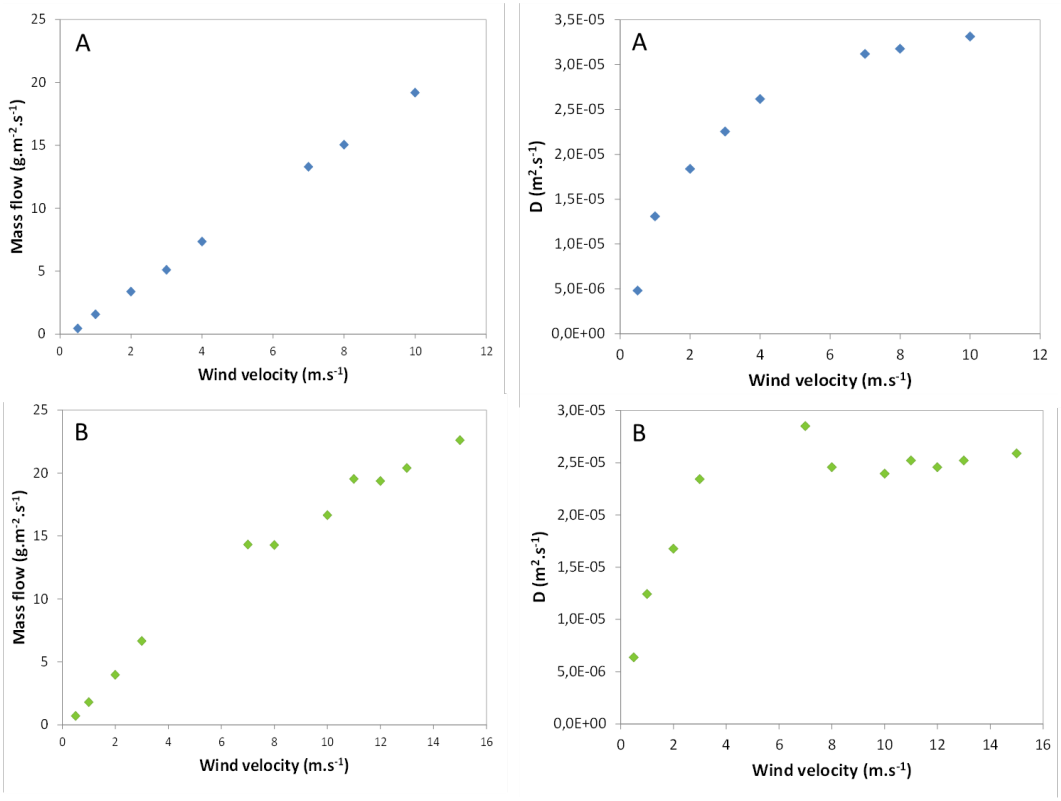

Figure 8. Mass flow and vapour diffusion coefficient with increasing wind velocities for acrylonitrile (A) and cyclohexane (B).

2. Comparison with model predictions

The observation and recording of experimental parameters allow for a thorough comparison of the collected data with the outputs from a simplified OSERIT version, while ensuring its inputs closely match the experimental conditions. When comparing experimental data collected for cyclohexane and acrylonitrile at various wind speeds with model simulations, a qualitative analysis of the initial results suggests that the model accurately predicts this evolution for both chemicals (Figure 9): as wind speed increases, so does the evaporation rate. However, this effect gradually diminishes with further increments in wind speed.

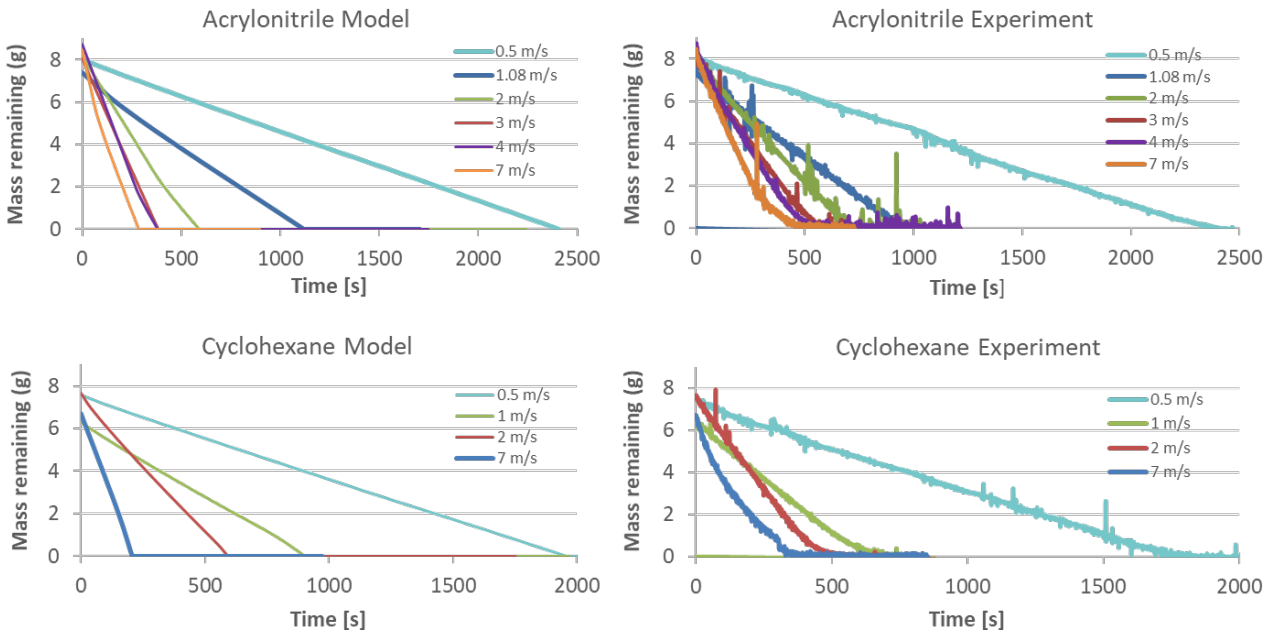

Figure 9. Comparison of the mass remaining between simulation (left) and observation (right) for acrylonitrile and cyclohexane at several wind speeds.

When looking more specifically at the evaporation rate for acrylonitrile at each wind speed tested, the accuracy of the model's prediction decreases as the wind speed increases (Figure 10). A similar

observation was made for cyclohexane, though the discrepancy between the model predictions and the observations is comparatively lower. In most case, a decrease of the evaporation rate was observed when almost all the chemical had evaporated, a phenomenon not reflected in the simulations. This could be due to the reduction of the slick area close to the end of the experiment, a factor not considered in the model. This is the case for all the other chemicals tested.

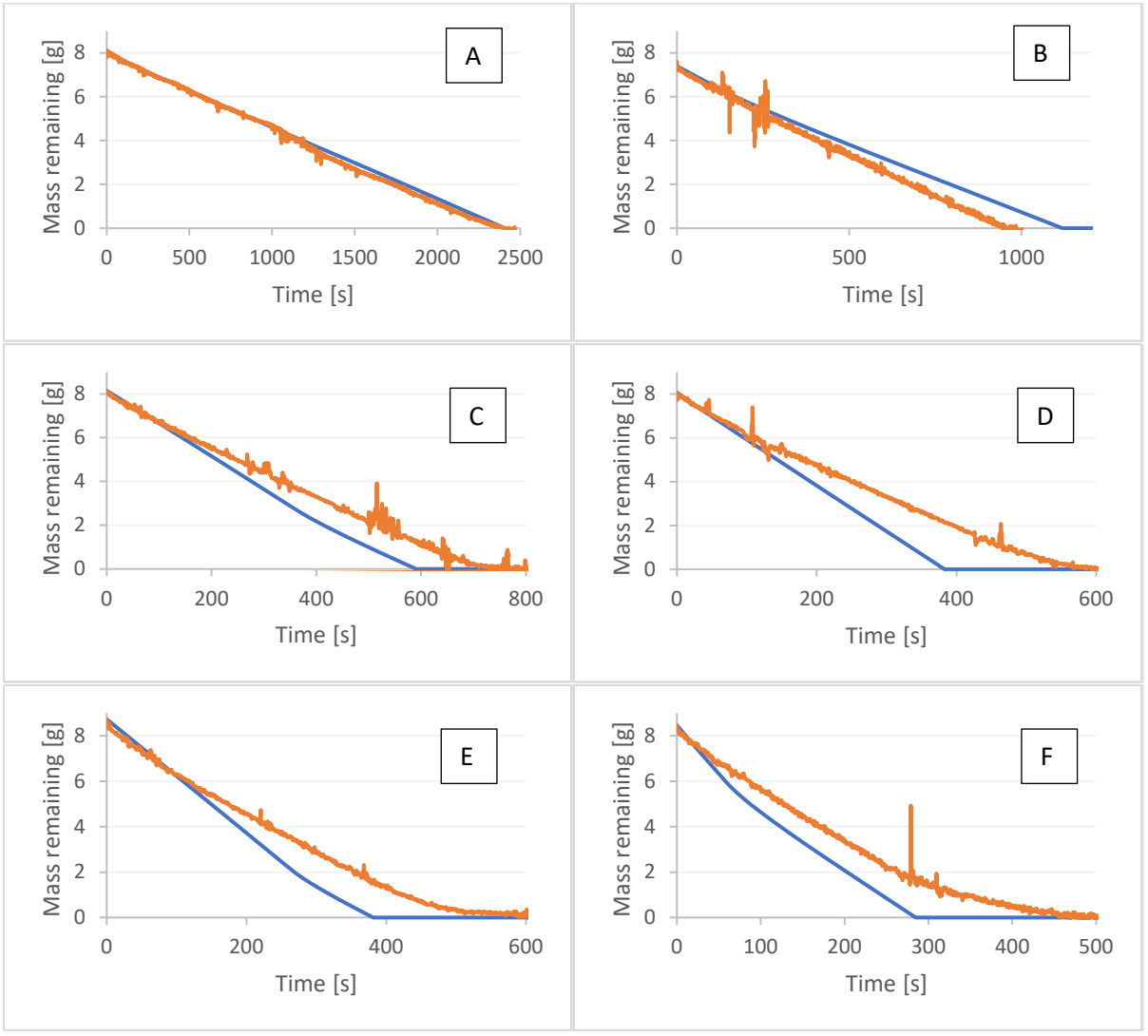

Figure 10: Comparison of the evaporation rate between simulation (blue line) and observation (orange line) for acrylonitrile at several windspeed (A:0.5 m/s, B:1.08 m/s, C:2m/s, D:3m/s, E:4m/s, F:7m/s)

Regarding vinyl acetate, only two repetitions of a single experiment conducted at a wind speed of 8 $m.s^{-1}$ are compared here (Figure 11). Similar to cyclohexane and acrylonitrile, there is a decrease in the rate of evaporation observed when the majority of the chemical has evaporated. Note that the two repetitions exhibit highly similar results in both the observations and the model outputs.

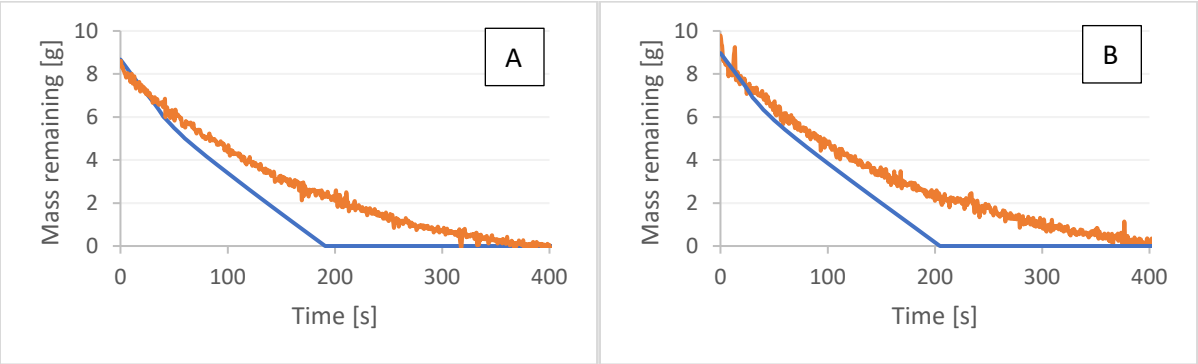

Figure 11: Comparison of the evaporation rate between simulation (blue line) and observation (orange line) for vinyl acetate at a wind speed of 8 $m.s^{-1}$ (2 repetitions).

CONCLUSIONS

Scientific aspects

The mechanisms driving the evaporation of a chemical from a slick were first investigated through experimental tests conducted in the wind tunnel developed by Cedre. Results showed that increasing wind velocities involve higher evaporation rates of chemicals, i.e. a faster evaporation of the slick. The evaporation process also transiently leads to a drop in liquid temperature. This temperature variation should not be so important in real environmental conditions due to external thermal exchange. The data collected were subsequently compared to the outputs of the simplified OSERIT model version. The OSERIT model is capable of accurately predicting the evaporation

rates of acrylonitrile, cyclohexane, and vinyl acetate in the wind tunnel, although differences between the model and observations are still present. However, it is likely that these differences fall within the uncertainty of wind speed estimates derived from meteorological forcing. As the chemical evaporates and the amount remaining in the dish decreases, it no longer covers the entire surface and starts to form droplets. This may explain the decrease in the evaporation rate at this stage, as the surface area decreases, an aspect not considered in the model. The growing disparity between the model and observations could potentially be attributed to an increasing influence of the petri dish on turbulence, as wind speed rises further. Moreover, due to the small size of the slick and its rapid evaporation, the actual surface temperature might be lower than the one recorded by the thermocouples. In particular, cyclohexane ice was observed at the highest wind speeds during the experiment. To address these issues, a new experiment could be performed with the chemical poured onto the surface of saltwater. This would help maintaining a more constant temperature for the slick through thermal exchange with the water, allowing for further testing of the competition between evaporation, dissolution, and volatilization. Subsequent investigations will also explore larger volumes (up to 500 mL) to enhance the scope and applicability of the study.

Operational aspects

This study has allowed to enhance the accuracy of existing evaporation models, providing crisis management stakeholders with more precise information for making critical decisions, especially in the assessment of toxic gas cloud formation (Go/No Go decisions). The OSERIT model is available at https://github.com/naturalsciences/weathering_module_4_marine_pollution. An application of the full OSERIT https://manifests-project.eu/. Note that in the event of an accidental

release of HNS in confined spaces such as in harbors, containing the slick with compatible booms can be the primary response to prevent its spread and slow down evaporation (some boom materials were tested for compatibility with corrosive HNS at Cedre and are fully suitable). Using available sorbent mats to cover the slick can further aid containment efforts. Additionally, deploying water curtains can help mitigate risks to the surrounding population by pushing away the gas cloud.

ACKNOWLEDGMENTS

The authors are grateful to the DG-ECHO of the European Commission for providing financial support to the MANIFESTS project.

REFERENCES

Bogeshwaran, K., Karunanithi, B., Tripuraneni, M., & Ross, S. J. (2015). Measurement and Correlation of Diffusion Coefficient In Hexane–Air System. *Measurement*, *11*(11), 19–31.

Bonn Agreement. (1994). Hazardous material spills. Counter pollution manual for incidents involving Hazardous and Noxious Substances (HNS). *London*.

Braconnier, R., Chaineaux, J., Triolet, J., Fontaine, J. R., & Salle, B. (2008). Mesures du flux d'évaporation de liquides volatils dans des ambiances de travail - INRS. *Hygiène et sécurité du travail*, (212), 1–11.

Cattafesta, L., Bahr, C., & Mathew, J. (2010). Fundamentals of wind-tunnel design. *Encyclopedia of Aerospace Engineering*, 1–10.

Cotte, L., Aprin, L., Prétat, C., Clémentine, K., Giraud, W., & Le Floch, S. (2023). D2.3 – Experimental study on evaporation from a chemical slick. *MANIFESTS project*, 1–63.

Decelle, L., & Nicolas, K. (2017). Conception d'une soufflerie de démonstration. *Projet de fin d'étude court. Polytech Lille*, 1–19.

Dulière, V., Ovidio, F., & Legrand, S. (2012). Development of an integrated software for forecasting the impacts of accidental oil pollution OSERIT. Royal Belgian Institute of Natural Sciences.

Gonczi, G. (2005). *Comprendre la thermodynamique* (Ellipses.).

Hamzah, H., Jasim, L. M., Alkhabbaz, A., & Sahin, B. (2021). Role of honeycomb in improving subsonic wind tunnel flow quality: Numerical study based on orthogonal grid. *Journal of mechanical Engineering Research and Developments*, *44*, 352–369.

Heymes, F., Aprin, L., Bony, A., Forestier, S., Cirocchi, S., & Dusserre, G. (2013). An experimental investigation of evaporation rates for different volatile organic compounds. *Process Safety Progress*, *32*(2), 193–198.

Jones, P. M., de Larrinaga, M. A. B., & Wilson, C. B. (1971). The urban wind velocity profile. *Atmospheric Environment (1967)*, *5*(2), 89–102.

Le Floch, S., Fuhrer, M., Merlin, F.-X., & Péron, O. (2011). *Experimental studies on the weathering of chemical products in open cells to predict their behaviour in case of a spill. Proceedings of International Oil Spill Conference (IOSC)*. Presentation made at the Proceedings of International Oil Spill Conference (IOSC).

Legrand, S., Poncet, F., Aprin, L., Parthenay, V., Donnay, E., Carvalho, G., Chataing-Pariaud, S., Dusserre, G., Gouriou, V., Le Floch, S., Le Guerroue, P., Hellouvry, Y.-H., Heymes, F., Ovidio, F., Orsi, S., Ozer, J., Parmentier, K., Poisvert, R., Poupon, E., Ramel, R., Schallier, R., Slangen, P., Thomas, A., Tsigourakos, V., Van Cappellen, M., & Youdjou, N. (2017). Modelling drift, behaviour and fate of HNS maritime pollution, HNS-MS final report, part II. Royal Belgian Institute of Natural Sciences; CEDRE; ARMINES, Ecole des Mines d'Alès; Alyotech France; Belgian FPS Health, food chain safety and environment.

Lepers, L., & Legrand, S. (2022). D4.2 – Improving the prediction of HNS concentration in the atmosphere. *MANIFESTS project*, 1–38.

Mackay, D., & Matsugu, R. S. (1973). Evaporation rates of liquid hydrocarbon spills on land and water. *The Canadian Journal of Chemical Engineering*, *51*(4), 434–439.

Mamaca, E., Girin, M., Le Floch, S., & el Zir, R. (2009). Review of chemical spills at sea and lessons learnt. A Technical Appendix to the INTERSPILL 2009 Conference White Paper "Are HNS spills more dangerous than oil Spills?"

Mamaca, E., Merlin, F., & Le Floch, S. (2004). Experimental studies on the weathering of chemicals in a field trial to predict their behaviour in case of a spill.

Purnell, K. (2009). Are HNS more dangerous than oil spills? *White paper for the interspill conference and 4th IMO R&D Forum*.

UNCTAD. (2017). Review of Maritime Transport 2017. *United Nations*, 1–137.

UNCTAD. (2022). Review of Maritime Transport 2022. *United Nations*, 1–195.